IOPscience iopscience.iop.org

Home Search Collections Journals About Contact us My IOPscience

Spintronics with multiferroics

This article has been downloaded from IOPscience. Please scroll down to see the full text article.

2008 J. Phys.: Condens. Matter 20 434221

(http://iopscience.iop.org/0953-8984/20/43/434221)

View the table of contents for this issue, or go to the journal homepage for more

Download details:
IP Address: 129.252.86.83
The article was downloaded on 29/05/2010 at 16:05

Please note that terms and conditions apply.

IOP PUBLISHING JOURNAL OF PHYSICS: CONDENSED MATTER

J. Phys.: Condens. Matter **20** (2008) 434221 (11pp) doi:10.1088/0953-8984/20/43/434221

Spintronics with multiferroics

H Béa[1], M Gajek[2], M Bibes and A Barthélémy

Unité Mixte de Physique CNRS/Thales, Route départementale 128, F-91767 Palaiseau, France
and
Université Paris-Sud, 91405 Orsay, France

E-mail: agnes.barthelemy@thalesgroup.com

Received 4 April 2008, in final form 1 July 2008
Published 9 October 2008
Online at stacks.iop.org/JPhysCM/20/434221

Abstract

In this paper, we review the recent research on the functionalization of multiferroics for spintronics applications. We focus more particularly on antiferromagnetic and ferroelectric $BiFeO_3$ and its integration in several types of architectures. For instance, when used as a tunnel barrier, $BiFeO_3$ allows the observation of a large tunnel magnetoresistance with Co and (La, Sr)MnO_3 ferromagnetic electrodes. Also, its antiferromagnetic and magnetoelectric properties have been exploited to induce an exchange coupling with a ferromagnet. The mechanisms of such an exchange coupling open ways to electrically control magnetization and possibly the logic state of spintronics devices. We also discuss recent results concerning the use of ferromagnetic and ferroelectric (La, Bi)MnO_3 as an active tunnel barrier in magnetic tunnel junctions with Au and (La, Sr)MnO_3 electrodes. A four-resistance-state device has been obtained, with two states arising from a spin filtering effect due to the ferromagnetic character of the barrier and two resulting from the ferroelectric behavior of the (La, Bi)MnO_3 ultrathin film. These results show that the additional degree of freedom provided by the ferroelectric polarization brings novel functionalities to spintronics, either as a extra order parameter for multiple-state memory elements, or as a handle for gate-controlled magnetic memories.

(Some figures in this article are in colour only in the electronic version)

1. Introduction

With their specificity to exhibit two coupled ferroic orders, multiferroics are a rare class of multifunctional materials. Within the original definition, the class of multiferroic materials only included compounds with two or more ferroic orders but the current trend is to extend it to materials with an antiferroic behavior [1], see figure 1. Ferroelectric materials in which the spontaneous electrical polarization can be switched by the application of an electric field are already largely used in the sensors industry or to design ferroelectric random access memories (FeRAM) in which the information is stored by the remanent polarization [2]. On the other hand, ferromagnetic materials, displaying a spontaneous magnetization that can be reversed by a magnetic field, have been used for a long time for data storage or magnetic field sensors. Furthermore, the research on magnetic multilayers, gave birth twenty years ago to a new electronics called spintronics that takes advantage not only of the charge of the carriers but also of their spins. The incorporation of multiferroic materials in the field of spintronics should allow one to take advantage of both functionalities (for example, ferromagnetism and ferroelectricity) independently but also to add new functionalities due to the coupling between the two orders. This magnetoelectric coupling between magnetism and ferroelectricity opens the way to control of the polarization by a magnetic field or that of the magnetization by an electric field. This coupling offers interesting perspectives for the design of ferroelectric memories with a non-destructive magnetic reading or magnetic random access memories (MRAM) with an electrical writing procedure (MERAM) [3, 4]. This should open the way to a better integration for these memories thanks to the local nature of the writing process. Multiferroic materials are scarce and almost all of them are antiferromagnet or weak ferromagnets [5]. The range of multiferroic systems can be broadened by designing artificial multiferroics combining ferromagnetic materials with large magnetostriction coefficient and ferroelectric or piezoelectric

[1] Present address: DPMC, University of Geneva, 24 Quai Ernest-Ansermet, CH 1211 Geneva, Switzerland.

[2] Present address: Department of Materials Science Engineering and Department of Physics, University of California, Berkeley, CA 94720, USA.

 © 2008 IOP Publishing Ltd Printed in the UK

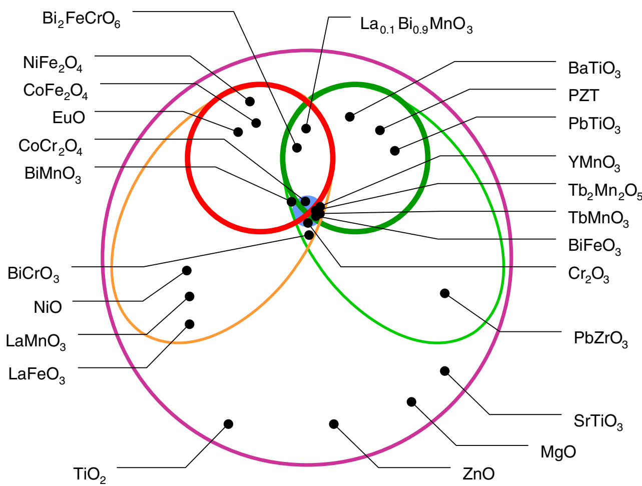

Figure 1. Classification of insulating oxides. The largest circle represents all insulating oxides among which one finds electrically polarizable materials (green ellipse) and magnetically polarizable materials (orange ellipse). Within each ellipse, the circle represents materials with a finite polarization (ferroelectrics) and/or a finite magnetization (ferro- and ferrimagnets). Depending on the definition, multiferroics correspond to the intersection between the ellipses or the circles. The small circle in the middle denotes systems exhibiting a magnetoelectric coupling. Inspired from [1].

materials (see, for example, [6–8]). In such artificial compounds, indirect magnetoelectric coupling is achieved mostly via the strain effect but more complex mechanisms could take place [9].

In this paper we will restrict ourselves to a few single phase multiferroics. We will review results on the functionalization of multiferroics for spintronics, with special focus on $BiFeO_3$ and (La, Bi)MnO_3 multiferroic thin films.

2. $BiFeO_3$: an antiferromagnetic ferroelectric at room temperature

Among multiferroic materials, $BiFeO_3$ (BFO) recently attracted a lot of attention because it is still the only established multiferroic with ordering temperatures far above room temperature (a key prerequisite for most applications). This rhombohedral perovskite has been studied since the late 1950s in its bulk form [10]. It was found to be ferroelectric up to 1100 K [11] with a polarization of 100 μC cm^{-2} lying along the [111] direction [12]. This compound is also a G-type antiferromagnet as deduced from Mössbauer spectroscopy and neutron diffraction experiments [13, 14]. Moreover, a superimposed cycloidal spin modulation was observed by neutron diffraction [15]. In the presence of this cycloidal modulation, a quadratic magnetoelectric effect has been measured, while when this cycloid is destroyed, for instance by applying a magnetic field of 20 T, a linear magnetoelectric effect occurs [16]. However, the precise microscopic mechanisms of the magnetoelectric effect in bulk $BiFeO_3$ are only now beginning to be understood [17].

In the following we report on the experiments we have performed in order to determine the potential of BFO thin films for spintronics. We report on the growth of BFO films by pulsed laser deposition, their structural and physical characterization and their use as barriers in tunnel junctions and in exchange-biased architectures.

2.1. Deposition and structure of $BiFeO_3$ thin films

The BFO films have been grown by pulsed laser deposition on (001)-oriented $SrTiO_3$ (STO) substrates using a frequency tripled (λ = 355 nm) Nd:YAG laser at a frequency of 2.5 Hz. BFO and 5%-Mn doped BFO (BFO–Mn) films were grown with an oxygen pressure of 6×10^{-3} mbar and a substrate temperature of 580 °C since these conditions allow the growth of single-phase films [18]. The $La_{2/3}Sr_{1/3}MnO_3$ (LSMO) and STO layers were deposited at 0.46 mbar of oxygen and a temperature of 700 °C, and the $SrRuO_3$ (SRO) film at an oxygen pressure of 0.1 mbar and a temperature of 700 °C. The targets are stoichiometric for LSMO, STO and SRO, while BFO and BFO–Mn targets contain 15% Bi excess, in order to compensate for its very high volatility.

The crystalline structure of BFO thin films on STO substrates with bottom electrodes (LSMO and SRO) has been studied by high resolution x-ray diffraction (XRD), using a Panalytical X'Pert PRO equipped with a Ge(220) monochromator. θ–2θ patterns, presented in figure 2(a), show the presence of (00l) peaks with l = 1–4 for the STO substrate, the BFO film and the SRO and LSMO bottom electrodes, indicating a (00l) texture of both bilayers on the substrate. In order to study the in-plane orientation of the films, we have measured ϕ scans around the $(30\overline{3})$ peaks of BFO and STO. For both bilayers, four peaks are obtained (not shown), separated by 90° and aligned with those of the substrate, indicating a cube-on-cube epitaxy of the bilayers. An example of such a peak is presented in figure 2(b) for the BFO/SRO bilayer.

The strain states of the bilayers have also been studied by performing reciprocal space mappings (RSM) around the (103) reflection as shown in figures 2(c) and (d) for the bilayers BFO/LSMO and BFO/SRO, respectively. These measurements allow the observation of three (103) peaks, one for the STO substrate, one for the BFO film and one for the bottom electrode, LSMO or SRO. All three peaks are aligned in the $q_{\parallel}$ direction, indicating that the in-plane parameter of the BFO and the bottom electrode are the same as the substrate lattice parameter. Both bilayers are thus fully strained on the STO substrate. The lattice parameters extracted from these x-ray data are a = 3.905 Å for all films, c = 4.10 Å for BFO in both bilayers, c = 3.84 Å for LSMO and c = 3.95 Å for SRO.

2.2. Ferroelectricity and magnetism of $BiFeO_3$ thin films

We focus now on the multiferroic properties of the BFO films, starting with their ferroelectric character. For ferroelectric polarization measurements, we used BFO–Mn films in order to decrease leakage currents [19]. Except from the leakage current, the physical properties, such as crystalline structure, are the same as the equivalent undoped BFO films [20]. We have measured polarization versus electric field by using a commercial TF Analyzer 2000 from aixACCT after sputtering 1000 μm^2 gold top electrodes through a shadow mask.

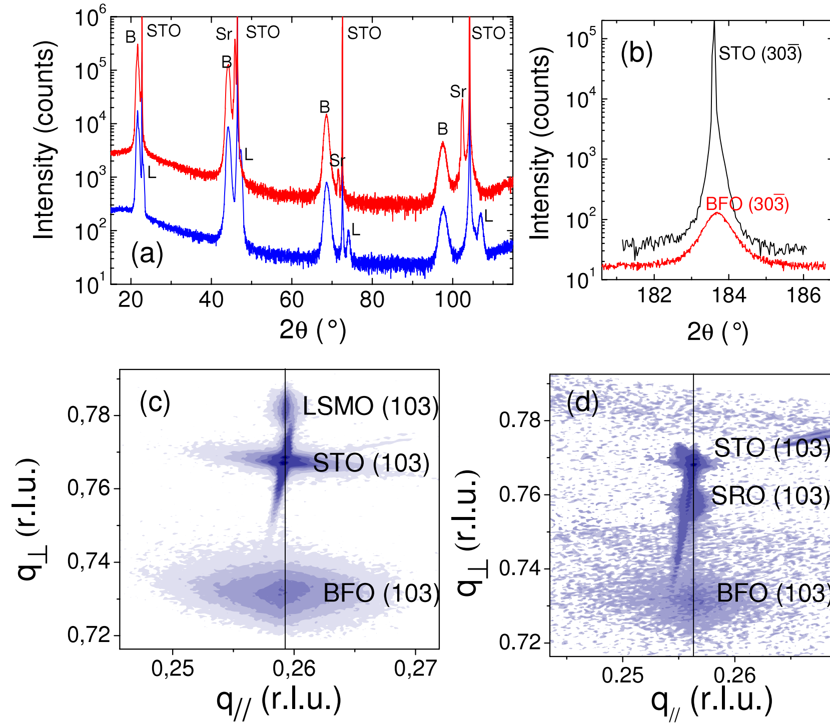

Figure 2. (a) θ–2θ x-ray diffraction pattern for 70 nm thick BFO films deposited on LSMO(11 nm) ∥ STO(001) (lower curve) and SRO(25 nm) ∥ STO(001) (upper curve). The peaks are attributed to STO for the substrate, B for the BFO film, Sr for the SRO layer and L for the LSMO film. (b) ϕ scan around (30$\bar{3}$) peak for a BFO(70 nm)/SRO(25 nm) ∥ STO(001) sample. RSM around (103) reflection for BFO(70 nm) films deposited on LSMO(11 nm) ∥ STO(001) (c) and SRO(25 nm) ∥ STO(001) (d).

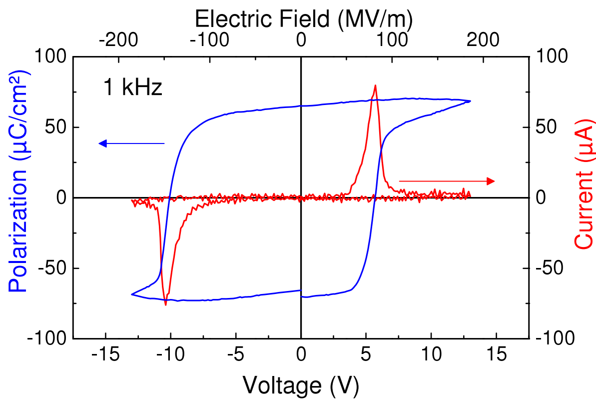

Figure 3. Polarization and current hysteresis loops versus voltage for a BFO–Mn(70 nm)/SRO ∥ STO(001) film measured at 1 kHz and at room temperature.

Figure 3 shows the polarization versus electric field for a BFO–Mn(70 nm)/SRO(35 nm) ∥ STO(001) sample measured at 1 kHz. A square hysteresis loop is obtained with no, or negligible, contribution from leakage currents. A remanent polarization of 65 μC cm^{-2} can be extracted from this measurement. This value is comparable to what was obtained in [001]-oriented thin films by other groups [21] and corresponds to a value of $\sim$100 μC cm^{-2} along the [111] direction, which is very close to the bulk value [12]. These results show the weak strain sensitivity of the polarization in BFO films, as is also shown in [22, 23] and predicted by Ederer and Spaldin [24]. This is in contrast with the strong strain effects reported in tetragonal ferroelectrics such as $PbTiO_3$ [24] or $BaTiO_3$ [25]. We emphasize that the large polarization of BFO thin films has led Fujitsu to use this material in next-generation FeRAMs [26]. We also note that this ferroelectric character is stable down to very small thicknesses [27].

We have also studied the magnetic order by neutron diffraction using the triple-axis 4F1 spectrometer at the Laboratoire Léon Brillouin (Saclay, France). Incident and final wavevectors were the same and chosen equal to $k_i = k_f = k = 1.55$ Å^{-1} or 1.20 Å^{-1}. A cold beryllium filter was placed in the scattered beam to avoid high-order contamination. The sample was placed in a vacuum can in order to minimize the background, and oriented so as to have [110]* and [001]* in the horizontal plane (* stands for reciprocal vector). Data shown in figure 4, taken at room temperature, presents measurements around $[\frac{1}{2}\,\frac{1}{2}\,\frac{1}{2}]^*$ and $[-\frac{1}{2}\,-\frac{1}{2}\,\frac{1}{2}]^*$ positions for a 240 nm thick BFO film deposited on STO(001). Magnetic Bragg peaks are clearly observed at these positions, indicating a doubling of the magnetic periodicity compared to the structural one in the [111] direction and thus in agreement with a G-type antiferromagnetic order, similar to bulk BFO.

We must, however, notice that no satellites, signature of the cycloidal modulation of the spins, are observed around the $[-\frac{1}{2}\,-\frac{1}{2}\,\frac{1}{2}]^*$ Bragg peak, in contrast to the measurements by Sosnowska *et al* [15] made on BFO powder. The absence of these satellites means that this cycloid is absent, or that the antiferromagnetic domains are too small for the cycloid to fully develop. In principle, the absence of a full cycloidal

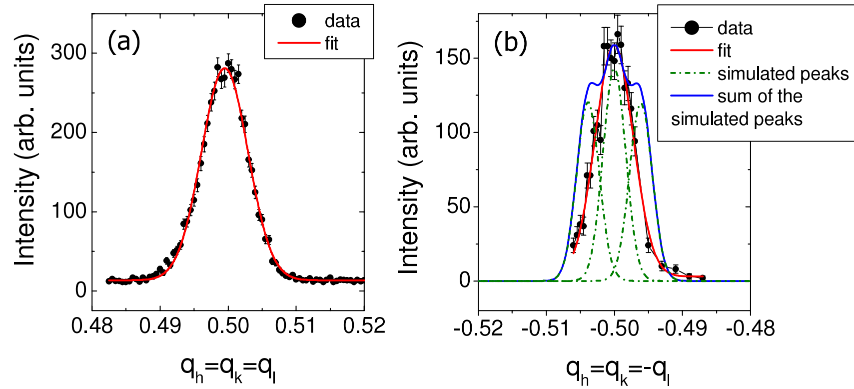

Figure 4. Neutron diffraction patterns of $[\frac{1}{2}\,\frac{1}{2}\,\frac{1}{2}]^*$ (a) and $[-\frac{1}{2}\,-\frac{1}{2}\,\frac{1}{2}]^*$ (b) measured along the [1 1 1]* and $[\bar{1}\,\bar{1}\,1]$ directions, respectively, for a 240 nm BFO film deposited on STO(001). The input and output collimation values are 60′. The wavevectors used are 1.55 $Å^{-1}$ (a) and 1.2 $Å^{-1}$ (b). The bold (red) line is a Gaussian fit to the data. In (b), the dotted lines are simulated main and satellite peaks. The sum of their intensities is shown as a solid (blue) line. For colors, see on-line.

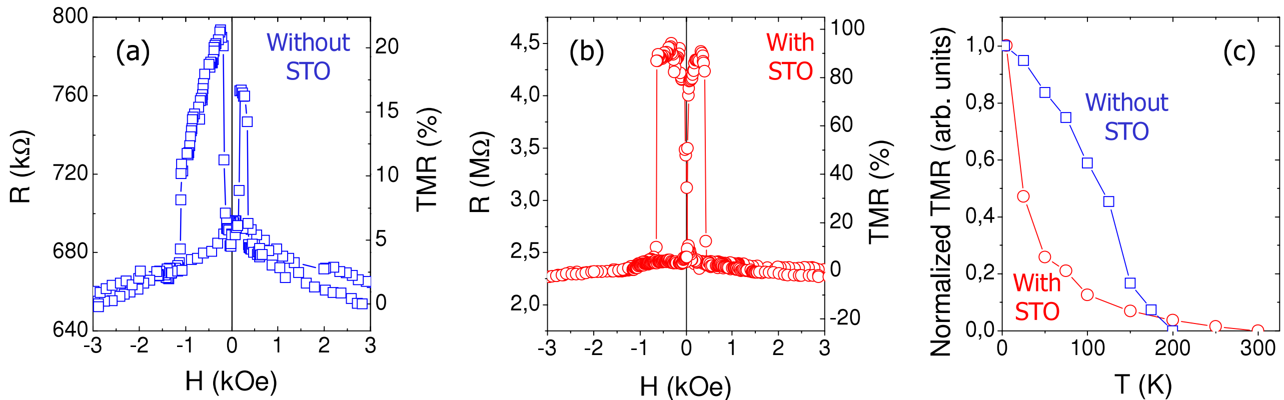

Figure 5. Resistance versus magnetic field for magnetic tunnel junctions with Co and LSMO ferromagnetic electrodes and multiferroic barriers measured at 3 K and 10 mV: (a) BFO(5 nm) single barrier, i.e. without STO and (b) BFO(2 nm)/STO(1.6 nm) double barrier, i.e. with STO. (c) Evolution of the TMR with temperature for these two junctions.

modulation in our films should allow the observation of the linear magnetoelectric effect that is averaged to zero when a coherent cycloid is present in the whole sample.

2.3. $BiFeO_3$ as a tunnel barrier in magnetic tunnel junctions

Being epitaxial, ferroelectric and antiferromagnetic (G-type), BFO films can be integrated as multiferroic elements into heterostructures. A first interesting application of such films is as tunnel barriers in magnetic tunnel junctions. Indeed, the electrical properties of ultrathin films were shown to be good enough to use BFO as tunnel barriers [28]. We have thus grown BFO(5 nm)/LSMO(11 nm) ∥ STO(001) and BFO(2 nm)/STO(1.6 nm)/LSMO(11 nm) ∥ STO(001) samples by pulsed laser deposition as explained previously. The STO ultrathin film was grown in the same conditions as LSMO in order to avoid its degradation as we will see later. CoO(12.5 nm)/Co(5 nm) was then sputtered on top of these samples [29]. A lithography was then made to define $5\times5\ \mu m^2$ junctions in the case of the single barrier and $50\times50\ nm^2$ junctions in the case of the double barrier.

Resistance versus magnetic field measurement for the single BFO barrier is presented in figure 5(a). Two resistance states are obtained as a function of the relative orientation of the magnetizations of the Co and LSMO ferromagnetic electrodes, thus corresponding to a tunnel magnetoresistance (TMR) effect that can be defined as a function of the resistance of the junction for the antiparallel (R_{AP}) and parallel (R_P) states and of the spin polarization (P_i) of the two ferromagnets as [30]

$$\mathrm{TMR} = \frac{R_{AP} - R_P}{R_P} = \frac{2P_1P_2}{1 - P_1P_2}. \quad (1)$$

Equation (1) leads to a value of the TMR around 20%, at 3 K and 10 mV. We must also notice that the TMR vanishes around 200 K, as presented in figure 5(c). This temperature corresponds to the Curie temperature (T_C) of the LSMO/BFO interface, which is lower by ∼100 K than the T_C of the LSMO film as measured in [28]. However, contrary to the magnetometry measurement probing the whole LSMO film [28], this transport measurement probes only a few monolayers in the LSMO close to the BFO barrier, from which the electrons tunnel. Indeed, during the BFO deposition, the

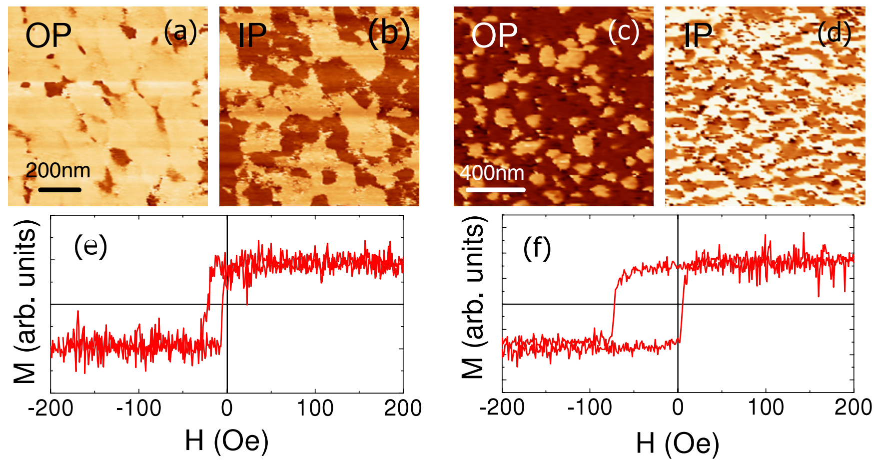

Figure 6. Out-of-plane ((a) and (c)) and in-plane ((b) and (d)) PFM images for 70 nm thick BFO films deposited on SRO ∥ STO(001) ((a) and (b)) and on SRO ∥ STO(111) ((c) and (d)). Magnetic hysteresis loops measured by AGFM for CoFeB(7.5 nm) layers deposited on BFO(70 nm)/SRO ∥ STO(001) (e) and BFO(70 nm)/SRO ∥ STO(111) (f). All measurements have been made at room temperature.

oxygen pressure is much lower than for LSMO deposition. A deoxygenation of the upper atomic layers of LSMO occurs and their magnetic and transport properties are then strongly modified and damaged [31].

In order to improve the LSMO properties, we have then deposited, before the BFO barrier, an STO protective layer under the same conditions as LSMO to avoid this deoxygenation. A TMR up to +100% is obtained at 3 K and 10 mV with this double barrier junction, as presented in figure 5(b). Moreover, the TMR remains up to ∼300 K, which is now close to the T_C of the LSMO film (see figure 5(c)). We can thus conclude that the introduction of the thin STO layer has improved the properties of the LSMO layer, leading to better transport properties.

The vanishing temperature of the TMR in this system being limited by the LSMO ferromagnetic electrode T_C, BFO has shown good potential to be used as a tunnel barrier due to the large TMR of +100% measured. Moreover, the positive sign of the TMR could be a signature of a symmetry filtering [32], as has been observed with MgO barriers [33, 34] that now leads to very high values at room temperature.

2.4. Use of the antiferromagnetism of $BiFeO_3$: exchange bias with a ferromagnet

As we have seen in section 2.2, BFO films present a G-type antiferromagnetic order as in the bulk. This antiferromagnetic order can be exploited to modify the magnetization of a ferromagnet through exchange bias. Moreover, due to the magnetoelectric coupling observed in BFO thin films [35], one may anticipate that the manipulation of the antiferromagnetic order in BFO could result in controlling the magnetization of the exchange-biased ferromagnet with an electric field [36], as has been initially reported by Borisov *et al* with the magnetoelectric Cr_2O_3 [42]. This might in turn give rise to electrically writable spintronics devices such as spin valves or magnetic tunnel junctions.

The phenomenon of exchange bias was discovered in CoO-embedded Co nanoparticles [37] in 1956 and consists in the widening and shifting of the magnetic hysteresis loop along the field axis in an antiferromagnetic/ferromagnetic system previously cooled under a magnetic field through the Néel temperature of the antiferromagnet. Several models have been developed to predict the amplitude of this exchange bias [38]. Among them, the Malozemoff model was found to describe quite well this phenomena in real systems [39]. In this model, the exchange bias, i.e. the horizontal shift in the hysteresis loop, varies as the inverse of the antiferromagnetic domain size.

Since the Néel temperature of BFO thin films is well above room temperature, an exchange bias at room temperature is induced on CoFeB ferromagnetic layers sputtered on top of a BFO film by applying a magnetic field during the CoFeB deposition [29]. In our case, the antiferromagnet is a multiferroic material presenting a magnetoelectric coupling, meaning that the antiferromagnetic domain size is linked to the ferroelectric one. In order to check the correspondence between the antiferromagnetic and ferroelectric domain size, we have measured them by neutron diffraction and piezoresponse force microscopy (PFM), respectively. The obtained values are comparable [40], suggesting the presence of a magnetoelectric coupling in our films. The existence of such magnetoelectric coupling could also be deduced from the fact that the size of the ferroelectric domain is closer to the typical magnetic domain size than to the ferroelectric one [41].

To go further and to better understand the mechanisms of this exchange bias with BFO, we have measured the ferroelectric domain configuration by using PFM, sputtered a CoFeB(7.5 nm) layer on top of the BFO film and measured its magnetic hysteresis loop by using an alternating gradient force magnetometer (AGFM). Results are presented in figure 6 for two different BFO samples with SRO bottom electrodes, one grown on STO(001) and the other on STO(111). A first observation is that the ferroelectric domain configuration is different for these two samples, probably due to different boundary conditions. For the sample deposited on STO(001) the average ferroelectric domain size is around 98 nm, while for the sample deposited on STO(111) this domain size is

lower, i.e. around 48 nm. The hysteresis loops of the CoFeB layer deposited on top of these two BFO films, as presented in figures 6(e) and (f), display a pronounced difference in exchange fields (i.e. −14.5 Oe for the (001)-oriented sample and −39 Oe for the (111)-oriented sample). From these two samples, and also from a larger dataset presented in [40], we can thus conclude that the exchange field varies as the inverse of the ferroelectric domain size, and that the Malozemoff model can be extended to this multiferroic/ferromagnetic system, due to the magnetoelectric coupling between the antiferromagnetic and ferroelectric domains.

Consequently, the modification of the ferroelectric domain configuration of the BFO by applying an electric field on the CoFeB or other ferromagnetic layer serving as the electrode would change also the antiferromagnetic domain configuration due to the magnetoelectric coupling. This will then affect the magnetic domain configuration of the ferromagnetic layer via the exchange coupling at the interface with the BFO. If such a ferromagnetic layer is part of a magnetoresistive device (spin valve or magnetic tunnel junction) this should allow one to obtain an electric drive of its resistance state [36]. Whereas the E field control of the BFO antiferromagnetic domain configuration [35] as well as the E field modification of the magnetization of a CoFe layer deposited on top of $BiFeO_3$ [43] have been reported, electrical control of the resistance of the device is still to be demonstrated. Such electrical control of the resistance has been reported in heterostructures combining the antiferromagnetic–ferroelectric $YMnO_3$ with a ferromagnetic layer of NiFe [44]. However, this is only observed at low temperature due to the low Néel temperature of this compound.

In summary, a polarization of 100 $\mu C\ cm^{-2}$, oriented along the [111] direction, very similarly to that of bulk BFO, has been measured in BFO thin films. Also, thin BFO films display the same G-type antiferromagnetic order as in the bulk [45] without the cycloidal modulation. Furthermore, a coupling between antiferromagnetic and ferroelectric domains has been observed [40, 41], thus making BFO thin films very attractive for applications, and particularly for a device displaying electric control of the magnetization.

3. $BiMnO_3$ and $(La, Bi)MnO_3$: a ferromagnetic ferroelectric

Another interesting multiferroic material for spintronics is $BiMnO_3$ (BMO) or $(La, Bi)MnO_3$ (LBMO). Indeed, this compound is one of the very few single-phase ferromagnetic and ferroelectric material whereas most of the multiferroic compounds are antiferromagnets or weak ferromagnets. Therefore, this compound offers the possibility to perform fundamental studies and test spintronics device concepts using a ferromagnetic ferroelectric. In its bulk form BMO has a heavily distorted perovskite structure belonging to the monoclinic space group $C2$, with $a = 9.5323$ Å, $b = 5.6064$ Å, $c = 9.8535$ Å and $\beta = 110.667$ [46, 47]. Few results have been reported in the literature on its ferroelectric character in bulk, probably due to the difficult preparation conditions (high pressure and temperature). A small polarization of the order of 100 $nC\ cm^{-2}$ has been measured on polycrystalline samples and thin films [48] with a ferroelectric Curie temperature reported around 450 K [48, 49]. Its ferromagnetic character, below 105 K [50], is due to an unusual orbital ordering triggered by the $6s^2$ electron lone pairs of Bi^{3+} [51]. This results in globally ferromagnetic superexchange and a magnetic moment of 3.6 μ_B/f.u. (i.e. 630 emu cm^{-3}) [52]. This unusual orbital ordering has been recently confirmed by neutron diffraction and resonant x-ray scattering experiments [47, 53].

Suggestion of the presence of a magnetoelectric coupling in this multiferroic compound arises from magnetocapacitance experiments by Kimura and coworkers [54] and modeling by Zhong *et al* [55]. This is characterized by the presence of an anomaly in the dielectric constant at the ferromagnetic Curie temperature that can be removed by restoring the magnetic order through application of a large magnetic field. Pure $BiMnO_3$ is difficult to achieve in bulk. Partial substitution of Bi by isovalent La allows stabilization, with only a little influence on the structural and magnetic properties at low La content (T_C is reduced to 95 K for 10% La [56]).

We have optimized the growth of $BiMnO_3$ and $(La, Bi)MnO_3$ layers and integrated them in heterostructures for spintronics. The results of this study are summarized in the following.

3.1. Deposition of $BiMnO_3$ and $(La, Bi)MnO_3$ thin films

A few groups have reported on the growth and properties of BMO thin films [57–60, 53]. We have grown $BiMnO_3$ (BMO) and 10% La-substituted BMO (LBMO) thin films on STO(001) substrates and LSMO or SRO ferromagnetic layers deposited on STO(001) substrates [61–63] by pulsed laser deposition using a KrF laser ($\lambda = 348$ nm) at a frequency of 2 Hz and with fluences ranging from 1.3 to 2.2 J cm^{-2}. A systematic study on the influence of the growth conditions on the properties of the films (i.e. temperature and growth pressure) has been performed. θ–2θ x-ray diffraction experiments showed the presence of Bi-rich parasitic phases at low temperature or high pressure. In contrast, at high temperature or low pressure, a hausmannite Mn_3O_4 phase is formed. Single-phase BMO or LBMO thin films are only obtained in a narrow range of pressure (5×10^{-2}–4×10^{-1} mbar) and temperature (600–650 °C) as shown in figure 1 of [63] by the phase diagram of LBMO thin films. This window is slightly enlarged in the case of LBMO compared to BMO, in good agreement with experiments on the bulk [56]. ϕ scans carried out on several reflections of the BMO or LBMO films indicate that the films are epitaxially grown and suggest that 30 nm LBMO film has a tetragonal unit cell even though its space group may have a lower symmetry [63] whereas reflections obtained for the 30 nm BMO films are compatible with the monoclinic symmetry [62]. ϕ scans also reveal a clear dependence of the out-of-plane parameter (from 3.97 to 3.94 Å) when the growth temperature is varied (from 600 to 650 °C) in the single-phase window whereas reciprocal space maps demonstrate the completely strained nature of the film with an in-plane parameter corresponding to the one of STO (3.905 Å).

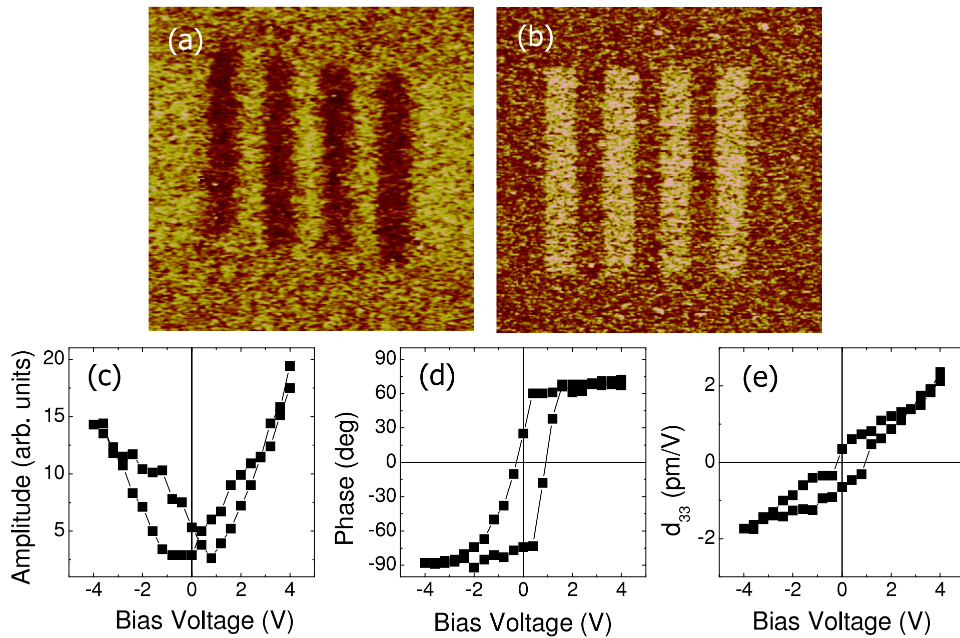

Figure 7. Out-of-plane PFM images for LBMO films of (a) 7 nm deposited on SRO ∥ STO(001) and (b) 2 nm deposited on LSMO ∥ STO(001). The images are $8 \times 8\ \mu m^2$. Amplitude (c), phase (d) and d_{33} (e) hysteresis loops measured on a 30 nm LBMO film deposited on LSMO ∥ STO(001). All measurements are made at room temperature.

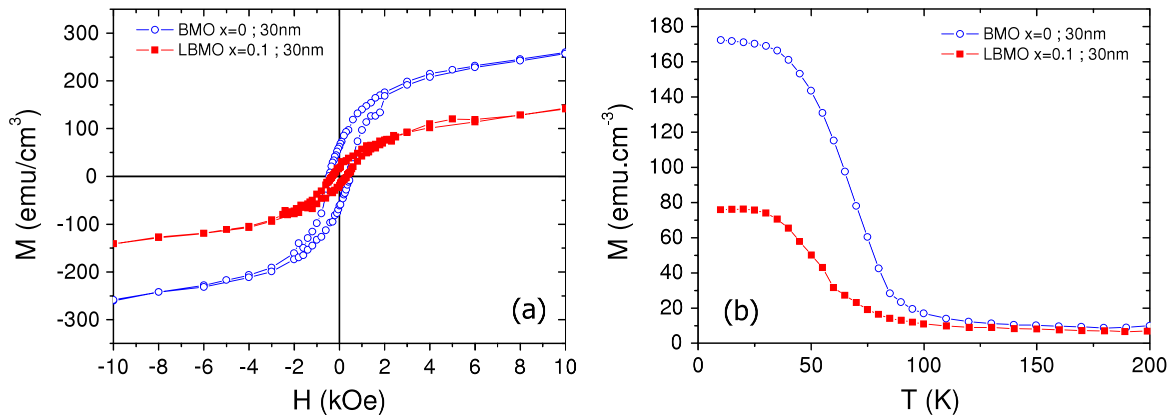

Figure 8. (a) Magnetization versus magnetic field for 30 nm BMO and LBMO ($x = 0.1$) films deposited on STO(001). The measurement is made at 10 K. (b) Variation of the magnetization with temperature for the same films measured under a magnetic field of 2 kOe.

3.2. Ferroelectric and magnetic properties of $BiMnO_3$ and $(La, Bi)MnO_3$ thin films

The ferroelectric nature of these films has been checked through piezoresponse force microscopy (PFM) experiments.

Figure 7(a) presents the results obtained after writing stripes with negative or positive DC bias on a 7 nm LBMO thin film on an SRO ∥ STO(001) template. The clear contrast between up and down domains, stable in time (at least over several hours), reflects the ferroelectric character of the compound. Remarkably, a similar contrast is observed on films as thin as 2 nm (see figure 7(b)) deposited on LSMO ∥ STO [64]. The ferroelectric character further confirmed by the piezoelectric phase versus electric-field curve presented in figure 7(d) which reveals the presence of two remanent polarization states in the film. From the amplitude (figure 7(c)) and phase (figure 7(d)) dependences we can reconstruct the dependence of the piezoelectric coefficient with the applied electric field (figure 7(e)) for this 30 nm LBMO thin film with LSMO electrode. The obtained hysteresis loop is not square, probably due to the small thickness of the film. A small piezoelectric coefficient of 2 pm V^{-1} is obtained at 4 V. This small value is in good agreement with the small polarization calculated [65] or observed [47] for the BMO system.

Magnetic properties of BMO and LBMO thin films are illustrated in figure 8 by the hysteresis loop and the temperature dependence of the magnetization of 30 nm films. In both cases a clear hysteresis loop is observed at low temperature and low field, pinpointing the ferromagnetic character. Nevertheless, the magnetization is smaller than in the bulk and not saturated even in a field as large as 5 T. This reduced magnetization is consistent with what has been observed by other groups

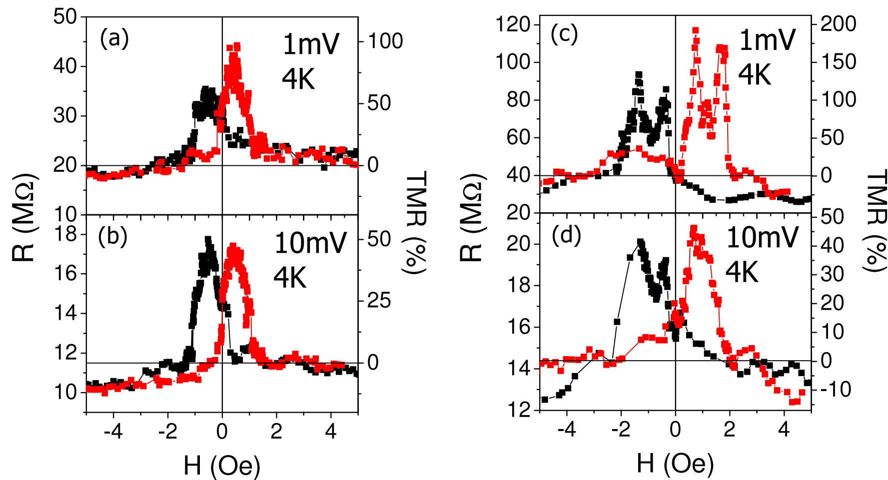

Figure 9. Variation of the junction resistance with magnetic field for a BMO(3.5 nm) barrier ((a) and (b)) and for an LBMO(3.5 nm) barrier ((c) and (d)). The measurements are made at 4 K with 1 mV bias ((a) and (c)) or 10 mV bias ((b) and (d)).

on BMO thin films [58, 59, 66]. The ferromagnetic Curie temperature, around 90 K in both cases (see figure 8(b)), is in good agreement with that of the bulk. We have attributed the smaller value of the magnetization as well as the existence of a slope in high magnetic field to the presence of Bi vacancies [63]. Such a presence of Bi vacancies is reflected by the decrease of the volume of the unit cell extracted from x-ray measurements. From the correlation between the magnetization and the unit cell volume, and considering a simple scenario taking into account that the occurrence of the Bi vacancies disrupts the orbital order at the origin of the ferromagnetism and results in the presence of Mn^{4+} ions antiferromagnetically coupled through superexchange to the Mn^{3+} matrix, we have been able to explain semi-quantitatively the experimental data. The antiferromagnetic ordering has been further demonstrated by x-ray magnetic circular dichroism experiments.

3.3. Towards the exploitation of the ferromagnetic and insulating character of (La, Bi)MnO_3

A first route to exploit the potential of these ferromagnetic and insulating compounds is to insert them as a ferromagnetic tunnel barrier, i.e. to design a spin filter. The concept of a spin filter was introduced by Esaki *et al* [67] and spin filter tunnel junctions were demonstrated by Moodera *et al* with EuS tunnel barriers [68]. It exploits a spin-dependent barrier height expected from the spin splitting of the energy bands in a ferromagnetic insulator. From the exponential dependence of the tunneling on the barrier height one can expect very efficient spin filtering. This filtering efficiency can be probed by adding a ferromagnetic counter electrode. Depending on the relative orientation of the magnetizations of the barrier and counter electrode, the current will be large or small, resulting in large tunnel magnetoresistance reflecting the spin filtering efficiency of the barrier. This has been confirmed, at least at low temperature, by the very high spin polarizations obtained by tunneling through barriers of EuS, EuSe and EuO [68–70]. Spin filtering tunnel barriers can be of great interest for spin injection into semiconductors without using ferromagnetic metals as spin-polarized injectors. Very large magnetoresistance effects can also be expected by switching from parallel to antiparallel the magnetic configuration of two spin filter barriers in a double junction [71]. In order to probe the potential of BMO and LBMO as a ferromagnetic barrier for spin filtering, ultrathin BMO and LBMO films were grown onto a STO(1 nm)/LSMO(25 nm) ∥ STO template. The intercalated 1 nm of the STO layer is used to magnetically decouple the BMO (or LBMO) barrier from the LSMO electrode and to preserve the half-metallic character of LSMO [72]. Conducting-tip atomic force microscopy (CT-AFM) experiments show an exponential increase of the resistance level with the thickness of the BMO or LBMO barrier in good agreement with the tunneling process. Small junctions 50 × 50 nm^2 were patterned by a nanolithography process based on the indentation of a thin resist by conductive-tip AFM, followed by the filling of the resulting hole with a sputtered Au layer [73]. In these experiments, the resistance of the LSMO bottom electrode was always small enough to ensure homogeneous current flow through the junction. $I(V)$ curves exhibit a clear nonlinear and asymmetric behavior expected for tunnel junctions with different electrodes. Typical $R(H)$ plots are presented in figure 9 for Au/BMO(3.5 nm)/STO(1 nm)/LSMO ((a) and (b)) and Au/LBMO(3.5 nm)/STO(1 nm)/LSMO ((c) and (d)) junctions for a bias of 1 mV (figures 9(a) and (c)) and 10 mV (figures 9(b) and (d)) applied to the junctions. The resistance maximum corresponds to the antiparallel configuration of the magnetization of LSMO and BMO or LBMO layers. The TMR amounts to 90% and 175% at 1 mV and 50% and 81% at 10 mV for BMO and LBMO tunnel barriers, respectively. The positive value of the TMR is in agreement with the calculated band structure of BMO [74, 65]. Using an extension of the Jullière model [30] (see equation (1)) where P_1 is the spin polarization of the ferromagnetic electrode (90% for a typical spin polarization of LSMO at the interface with STO at a bias of 10 mV [75]) and P_2 is the spin filtering efficiency of the ferromagnetic barrier, one finds a spin filter efficiency of

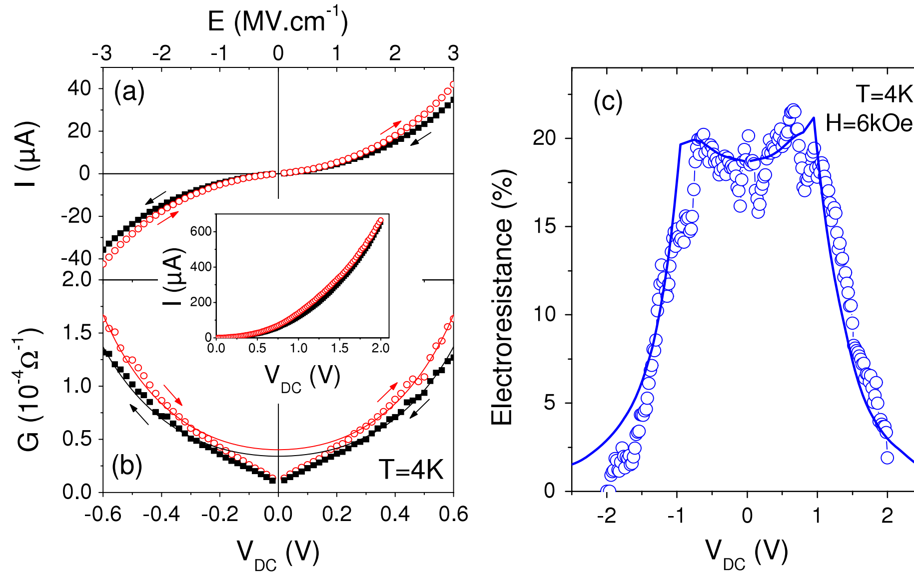

Figure 10. Current (a) and conductance (b) variations with the bias for increasing and decreasing voltages for an Au/LBMO(2 nm)/LSMO junction measured at 4 K under 6 kOe. The curves are fits of the conductance. In the inset is the current versus bias in the 0–2 V range. (c) Variation of the ER. The curve is the result of a simulation (see text).

22% and 36% for BMO and LBMO, respectively. A very fast and symmetric decrease of the TMR effect with the bias is observed in all the junctions [61] as already shown in other spin filters [76]. This symmetric drop has been ascribed to magnon excitations inside the ferromagnetic barrier. Smaller values of the TMR are obtained when no STO spacer is inserted. This less important value can be ascribed to some coupling between the ferromagnetic LSMO electrode as reflected by a less well-defined antiparallel state (see figure 11) but also the smaller value of the spin polarization of LSMO at the interface with BMO or LBMO tunnel barrier.

3.4. Influence of the ferroelectric character of the (*La*, *Bi*)MnO_3 *ferromagnetic barrier: towards the exploitation of multifunctionality.*

The ferroelectric character of the LBMO compound is expected to influence the tunneling properties. The influence of the electrical polarization on tunneling has been investigated experimentally [77] and theoretically [78–80] in ferroelectric junctions. A first mechanism leading to a modulation of the tunnel current by the polarization of the barrier is the variation of the barrier thickness due to the converse piezoelectric effect. This mechanism gives rise to asymmetrical $I(V)$ curves with a shift of the conductance minimum to a non-zero voltage [79]. A second mechanism is related to the presence of charges at the interfaces associated with the ferroelectric polarization and the different charge screening at the electrode–barrier interfaces if two different materials, with different screening lengths, are used as electrodes. This screening controls the depolarizing field across the junction and therefore the profile of the barrier potential seen by the tunneling electrons [78]. Using electrodes with different screening lengths results in asymmetric deformation of the barrier potential profile induced by the ferroelectric polarization and different average barrier heights for different orientations of the polarization.

From the low d_{33} value estimated by PFM, the first mechanism will result in a negligible shift of only 3.6 mV. In our case, the electrodes are Au and LSMO for which screening lengths of 0.07 nm and 0.2–1.9 nm [81, 82], respectively, have been reported. The second mechanism is thus likely to be active in our LBMO-based junctions. The influence of the ferroelectric character of the LBMO barrier appears on the $I(V)$ curves obtained at 6 kOe by cycling the bias voltage between + and −2 V in an Au/LBMO(2 nm)/LSMO junction (see figure 10(a)). A noticeable hysteresis is observed: the tunneling current is smaller (larger) for a given voltage when the voltage is swept from +2 to −2 V (from −2 to +2 V). This is even clearer on the voltage dependence of the conductance $G = \mathrm{d}I/\mathrm{d}V$ (figure 10(b)) where a shift along the vertical axis is observed. No shift along the abscissa axis is observed, in good agreement with the negligible value of the piezoelectric coefficient. The hysteresis in the $I(V)$ curves corresponds to an electroresistance (ER) effect that we define as the normalized difference between the $I(V)$ curves for increasing and decreasing voltage (see figure 10(c)): ER = $[I_{(V<0\to V>0)} - I_{(V>0\to V<0)}]/I_{(V>0\to V<0)}$. Such ER phenomena has been observed for different values of the magnetic field and in several junctions. It is reproducible and does not depend on the voltage sweep rate. As shown in figure 10(c), the ER amounts to 22%. The amplitude of the effect increases with the maximum applied voltage in agreement with a $P(E)$ loop hard to saturate. In the bias dependence of this ER phenomena, we can distinguish a low voltage regime where the ER is roughly constant, and a symmetric high-voltage regime in which the ER decreases rapidly to zero. Considering the mechanism proposed by Zhuravlev *et al* [78] and assuming that the $P(E)$ loop of the ferroelectric barrier is hard to saturate, as can be inferred from the d_{33} versus E shown in figure 7(e),

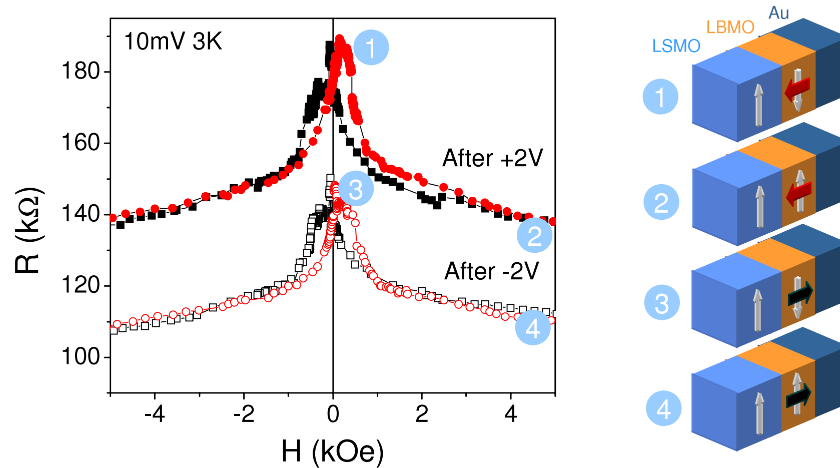

Figure 11. Variation of the resistance of an Au/LBMO(2 nm)/LSMO junction as a function of the magnetic field and previous applied bias displaying four resistance states whose magnetic and electric configurations are represented on the right-hand side.

we can account for the bias dependence of the conductances and that of the ER effect (see the good agreement between the line corresponding to the model and the experimental data in figure 10(c)). Finally, it is possible to combine both the ER and TMR effect to obtain four different resistance states at low bias voltage (see figure 11). Two of these states are related to the relative orientation of the magnetizations of the barrier and LSMO counter electrode, whereas the two others are related to the orientation of the ferroelectric polarization which modulates the barrier height. Our junctions based on a multiferroic tunnel barrier therefore define a four-resistance-state system in which it is possible to cycle between the different states via the application of a magnetic and/or electric field [64].

4. Conclusions

We have reviewed here the functionalization of multiferroic materials for spintronics applications. First, ferroelectric and antiferromagnetic $BiFeO_3$ thin films have been used as tunnel barriers thanks to their epitaxial and insulating properties. A large tunnel magnetoresistance has been observed. Moreover, one can take advantage of their antiferromagnetic, multiferroic and magnetoelectric properties to induce an exchange bias with a ferromagnetic CoFeB layer. The understanding of the mechanisms of this exchange coupling, which follows the Malozemoff model, paves the way towards electrical control of the magnetization of the ferromagnet, which could solve the writing problem in magnetic memories (MRAM).

On the other hand $BiMnO_3$ and (La, Bi)MnO_3 thin films that are both ferroelectric and ferromagnetic below 100 K have been used as active tunnel barriers. Indeed, their insulating and ferromagnetic properties allowed the measurements of a tunnel magnetoresistance due to a spin filtering effect through the barrier in Au/BMO (or LBMO)/LSMO magnetic tunnel junctions. Moreover, the ferroelectric behavior of LBMO ultrathin films, which remains down to 2 nm, has been used to modify the resistance state of this magnetic tunnel junction by the application of an electric field that changes its ferroelectric state. This defines a four-resistance-state device that is very interesting for increasing the storage density in memories.

Acknowledgments

We thank K Bouzehouane, S Fusil, E Jacquet, C Deranlot, S Petit, M Varela and J Fontcuberta. This study was partially supported by the EU STREPs Nanotemplates (Contract NMP-2004-505955) and MaCoMuFi (Contract FP6-NMP3-CT-2006-033221), the European Science Foundation THIOX network, the Picasso France-Spain project (EGIDE), the project FEMMES of the French Agence Nationale de la Recherche and the Conseil Général de l'Essone.

References

[1] Eerenstein W, Mathur N D and Scott J F 2006 *Nature* **442** 759
[2] Dawber M, Rabe K M and Scott J F 2005 *Rev. Mod. Phys.* **77** 1083
[3] Bibes M and Barthélémy B 2008 *Nat. Mater.* **7** 425
[4] Chen X, Hochstrat A, Borisov P and Kleeman W 2006 *Appl. Phys. Lett.* **89** 202508
[5] Hill N A 2000 *J. Phys. Chem.* B **104** 6694
[6] Lee M K, Nath T K, Eom C B, Smoak M C and Tsui F 2000 *Appl. Phys. Lett.* **77** 3547
[7] Zavaliche F *et al* 2005 *Nano Lett.* **5** 1793
[8] Eerenstein W, Wiora M, Prieto J L, Scott J F and Mathur N D 2007 *Nat. Mater.* **6** 348
[9] Duan C G, Jaswal S S and Tsymbal E Y 2006 *Phys. Rev. Lett.* **97** 047201
[10] Royen P and Swars K 1957 *Angew. Chem.* **69** 779
[11] Smolenskii G A, Yudin V M, Sher E S and Stolypin Y E 1963 *Sov. Phys.—JETP* **16** 622
[12] Lebeugle D, Colson D, Forget A and Viret M 2007 *Appl. Phys. Lett.* **91** 022907
[13] Kiselev S V, Ozerov R P and Zhdanov G D 1963 *Sov. Phys.—Dokl.* **7** 742
[14] Bhide V G and Multani M S 1965 *Solid State Commun.* **3** 271
[15] Sosnowska I, Peterlin-Neumaier T and Steichele E 1982 *J. Phys. C: Solid State Phys.* **15** 4835–46
[16] Popov Yu F, Zvezdin A K, Vorob'ev G P, Kadomtseva A M, Murashev V A and Rakov D N 1993 *JETP Lett.* **57** 69

[17] Lebeugle D, Colson D, Forget A, Viret M, Bataille A M and Gukasov A 2008 *Phys. Rev. Lett.* **100** 227602
[18] Béa H *et al* 2005 *Appl. Phys. Lett.* **87** 072508
[19] Singh S K, Ishiwara H and Maruyama K 2006 *Appl. Phys. Lett.* **88** 262908
[20] Zhu X H, Béa H, Bibes M, Fusil S, Bouzehouane K, Jacquet E and Barthélémy A 2008 *Appl. Phys. Lett.* submitted
[21] Wang J *et al* 2003 *Science* **299** 1719
[22] Bai F, Wang J, Wuttig M, Li J, Wang N, Pyatakov A P, Zvezdin A K, Cross L E and Viehland D 2005 *Appl. Phys. Lett.* **86** 032511
[23] Kim D H, Lee H N, Biegalski M D and Christen H M 2008 *Appl. Phys. Lett.* **92** 012911
[24] Ederer C and Spaldin N A 2005 *Phys. Rev. Lett.* **95** 257601
[25] Choi K J *et al* 2004 *Science* **306** 1005
[26] http://www.fujitsu.com/my/news/pr/fmal_20060808.html.
[27] Béa H, Fusil S, Bouzehouane K, Bibes M, Sirena M, Herranz G, Jacquet E, Contour J-P and Barthélémy A 2006 *Japan. J. Appl. Phys.* **L187** 45
[28] Béa H *et al* 2006 *Appl. Phys. Lett.* **88** 062502
[29] Béa H *et al* 2006 *Appl. Phys. Lett.* **89** 242114
[30] Jullière M 1975 *Phys. Lett.* A **54** 225
[31] Viret M, Drouet M, Nassar J, Contour J-P, Fermon C and Fert A 1997 *Europhys. Lett.* **39** 545
[32] Béa H, Bibes M, Basletic M, Herranz G, Guillemet R, Bouzehouane K, Fusil S and Barthélémy A 2008 in preparation
[33] Parkin S S P, Kaiser C, Panchula A, Rice P M, Hughes B, Samant M and Yang S-H 2004 *Nat. Mater.* **3** 862
[34] Yuasa S, Fukushima A, Kubota H, Suzuki Y and Ando K 2006 *Appl. Phys. Lett.* **89** 042505
[35] Zhao T *et al* 2006 *Nat. Mater.* **5** 823
[36] Binek C and Doudin B 2005 *J. Phys.: Condens. Matter* **17** L39
[37] Meiklejohn W P and Bean C P 1956 *Phys. Rev.* **102** 1413
[38] Nogués J and Schuller I K 1999 *J. Magn. Magn. Mater.* **192** 203
[39] Malozemoff A P 1987 *Phys. Rev.* B **35** 3679
[40] Béa H, Bibes M, Ott F, Dupé B, Zhu X-H, Petit S, Fusil S, Deranlot C, Bouzehouane K and Barthélémy A 2008 *Phys. Rev. Lett.* **100** 017204
[41] Catalan G, Béa H, Fusil S, Bibes M, Paruch P, Barthélémy A and Scott J F 2008 *Phys. Rev. Lett.* **100** 027602
[42] Borisov P, Hochstrat A, Chen X, Kleemann W and Binek Ch 2005 *Phys. Rev. Lett.* **94** 117203
[43] Chu Y-H *et al* 2008 *Nat. Mater.* **7** 478
[44] Laukhin V *et al* 2006 *Phys. Rev. Lett.* **97** 227201
[45] Béa H, Bibes M, Petit S, Kreisel J and Barthélémy A 2007 *Phil. Mag. Lett.* **87** 165
[46] Atou T, Chiba H, Ohoyama K, Yamagauchi Y and Syono Y 1999 *J. Solid State Chem.* **145** 639
[47] Moreira dos Santos A F, Cheetham A K, Atou T, Syono Y, Yamaguchi Y, Ohoyama K, Chiba H and Rao C N R 2002 *Phys. Rev.* B **66** 064425
[48] Moreira dos Santos A F, Parashar S, Raju A R, Zhao Y S, Cheethan A K and Rao C N R 2002 *Solid State Commun.* **122** 49
[49] Chi Z H, Xiao C J, Feng S M, Li F Y, Jina C Q, Wang X H, Chen R Z and Li L T 2005 *J. Appl. Phys.* **98** 103519
[50] Sugawara F, Iida S, Syono Y and Akimoto A 1968 *J. Phys. Soc. Japan* **25** 1553
[51] Seshadri R and Hill N A 2001 *Chem. Mater.* **13** 2892
[52] Chiba H, Atou T and Syono Y 1997 *J. Solid State Chem.* **132** 139
[53] Yang C-H, Koo J, Song C, Koo T Y, Lee K B and Jeong Y H 2006 *Phys. Rev.* B **73** 224112
[54] Kimura T, Kawamoto S, Yamada I, Azuma M, Takano M and Tokura Y 2003 *Phys. Rev.* B **67** 180401R
[55] Zhong C, Fang J and Jiang Q 2004 *J. Phys.: Condens. Matter* **16** 9059
[56] Troyanchuk I O, Mantyskaja O S, Szymczak H and Shvedun M Y 2002 *Low Temp. Phys.* **28** 569
[57] Son J Y, Kim B G, Kim C H and Cho J H 2004 *Appl. Phys. Lett.* **84** 4971
[58] Eerenstein W, Morrison F D, Scott J F and Mathur N D 2005 *Appl. Phys. Lett.* **87** 101906
[59] Oshima E, Saya Y, Nantoh M and Kawai M 2000 *Solid State Commun.* **116** 73
[60] Moreira dos Santos A F, Cheetham A K, Tian W, Pan X, Jia Y, Murphy N J, Lettieri J and Schlom D G 2004 *Appl. Phys. Lett.* **84** 91
[61] Gajek M, Bibes M, Barthélémy A, Bouzehouane K, Fusil S, Varela M, Fontcuberta J and Fert A 2005 *Phys. Rev.* B **72** 020406R
[62] Gajek M, Bibes M, Barthélémy A, Bouzehouane K, Fusil S, Varela M, Fontcuberta J and Fert A 2005 *J. Appl. Phys.* **97** 103909
[63] Gajek M, Bibes M, Wyczick F, Varela M, Fontcuberta J and Barthélémy A 2007 *Phys. Rev.* B **75** 174417
[64] Gajek M, Bibes M, Fusil S, Bouzehouane K, Fontcuberta J, Barthélémy A and Fert A 2007 *Nat. Mater.* **6** 296
[65] Shishidou T, Mikamo N, Uratani Y, Ishii F and Oguchi T 2004 *J. Phys.: Condens. Matter* **16** S5677
[66] Yang C H, Koo T Y, Lee S H, Song C, Lee K B and Jeong Y H 2006 *Europhys. Lett.* **74** 348
[67] Esaki L, Stiles P J and von Molnar S 1967 *Phys. Rev. Lett.* **19** 852
[68] Moodera J S, Hao X, Gibson G A and Meservey R 1988 *Phys. Rev. Lett.* **61** 637
[69] Moodera J S, Meservey R and Hao X 1993 *Phys. Rev. Lett.* **70** 853
[70] Santos T S and Moodera J S 2004 *Phys. Rev.* B **69** 241203R
[71] Worledge C and Geballe T H 2000 *J. Appl. Phys.* **88** 5277
[72] Bowen M, Bibes M, Barthélémy A, Contour J-P, Anane A, Lematre Y and Fert A 2003 *Appl. Phys. Lett.* **82** 233
[73] Bouzehouane K, Fusil S, Bibes M, Carrey J, Blon T, Le D M, Seneor P, Cros V and Vila L 2003 *Nano Lett.* **3** 1599
[74] Hill N A and Rabe K M 1999 *Phys. Rev. Lett.* **59** 859
[75] Bowen M, Barthélémy A, Bibes M, Jacquet E, Contour J P, Fert A, Ciccaci F and Bertacco R 2005 *Phys. Rev. Lett.* **95** 137203
[76] Lüders U, Bibes M, Fusil S, Bouzehouane K, Jacquet E, Sommers C B, Contour J P, Bobo J F, Barthélémy A, Fert A and Levy P M 2007 *Phys. Rev.* B **76** 164412
[77] Rodriguez Contreras J, Kohlstedt H, Poppe U, Waser R, Buchal C and Pertsev N A 2003 *Appl. Phys. Lett.* **83** 4595
[78] Zhuravlev M Ye, Sabirianov R F, Jaswal S S and Tsymbal E Y 2005 *Phys. Rev. Lett.* **94** 246802
[79] Kohlstedt H, Pertsev N A, Rodriguez-Contreras J and Waser R 2005 *Phys. Rev.* B **72** 125341
[80] Tsymbal E Y and Kohlstedt H 2006 *Science* **313** 181
[81] Hong X, Posadas A and Ahn C H 2005 *Appl. Phys. Lett.* **86** 142501
[82] Dzero M, Gorkov L P and Kresin V Z 2003 *Int. J. Mod. Phys.* B **17** 2095